Biogenic surfactant mediated facile synthesis of visible light sensitized Zn/Mg co-doped TiO2 Nanomaterials– A Green approach: Evaluation of photocatalytic activity by degradation of Amido Black 10B

Siva Rao Tirukkovalluri (sivaraoau@gmail.com)
Andhra University https://orcid.org/0000-0001-5156-1885
Genji Jaishree
Andhra University College of Science and Technology
Gorli Divya
Andhra University College of Science and Technology
M.L.V. Prasanna Chippada
Andhra University College of Science and Technology
Imandi Manga Raju
Andhra University College of Science and Technology

Research Article

Keywords: Zn/Mg-codoped TiO2, Sapindus emerginatus, biogenic extract, Amido Black 10B, Visible light Photodegradation

Posted Date: February 8th, 2022

DOI: https://doi.org/10.21203/rs.3.rs-1239703/v1

Abstract

Visible light driven Zn and Mg co-doped TiO_2 nanomaterials were synthesized by varying dopant concentrations in presence of biogenic surfactant *Sapindus emerginatus* biogenic extract via Solgel method and has been successfully applicated to the degradation of Amido Black 10B, an exemplary anionic textile azo dye pollutant. In this study, explored the potent capping properties of biogenic extract surfactant by encapsulating the Zn/Mg co-doped TiO_2. In a view to assess the physical and optical properties of as synthesized catalyst, various advanced instrumental techniques were adopted. The Transmission Electron Microscopy and Scanning Electron Microscopy analysis shows the formation of small particle size (6.92 nm) and rough surface respectively pertaining to ZMT4S2. The substitutional doping of Zn and Mg into TiO_2 framework by substituting Ti^{4+} ion and the encapsulation of surfactant around catalyst was confirmed by Fourier Transform-Infrared Spectroscopy (FTIR) spectral studies. The surface area of the ZMT4S2 was found to be high (195.20 $m^2\ g^{-1}$) as compared with undoped TiO_2 (32.50 $m^2\ g^{-1}$) and ZMT4 (7.02 $m^2\ g^{-1}$). The red shift in the absorbance was observed for all the catalysts analyzed using UV-DRS making them active in visible region with maximum shift corresponds to a band energy difference of 2.1 eV for ZMT4S2. The sensitivity of the catalyst towards visible light was confirmed by its band gap energy measurement using UV-vis DRS. The anatase phase of all the catalysts were confirmed using Powder X-ray diffraction. The composition and wt% of dopants revealed the EDX spectra agrees well with the calculated value. The slightly shifted frequency bands (FTIR) further confirmed the doping of Zn and Mg. The characterization analysis reports further accounts for the effective degradation of AB10B dye (99%) taking place within 20 min of irradiation time at optimized reaction parameters such as best dopant concentration ZMT4, catalyst dosage (100 mgL^{-1}), dye concentration (10 mgL^{-1}) and solution pH 3.

1. Introduction

The benchmark photocatalyst, titanium dioxide (TiO_2) in anatase form has been endorsed for its suitability towards photocatalytic processes for effective removal of textile dye pollutants in aqueous medium due to its strong oxidizing power, long-term stability, non-photocorrosive nature, etc. [1]. Even after rectifying the bandgap and electron hole recombination of TiO_2 by co-doping with Metal/Nonmetal or Metal/Metal [2], the rate of photocatalytic activity of the catalyst is still not satisfactory. To insight into this problem, many researchers have designed various methods to make a specific modification in TiO_2 to reduce the band gap, electron hole recombination [2] and increase the surface area [3] by applying different combinations of dopants and capping agent respectively.

Zhuang et al. worked on the synthesis of Sn and N co-doped TiO_2 via sol–gel method through post-nitridation route at 500°C for 20 h [4]. Abhijeet et al. noticed that samples annealed at a quite high temperature for a long time (20 h), results in decrease in specific surface area and photocatalytic activity owing to increase in the particle size. So, he reported the synthesis of Sn doped N-TiO_2 nanoparticles microwave assisted method by a greener approach [5]. Ravikumar et al reported the synthesis Zn and B-

codoped TiO_2 and found effective for acid red degradation [6]. Although Nonmetal doping of TiO_2 can cause red shift of TiO_2 making it responsive towards visible light, however during the annealing process, doped nonmetal content decreases [7] and as a result, the oxidizing ability of the TiO_2 nanocrystalline phase is diminished in turn leads to decrement in photocatalytic activity.

Based on the above facts various research group have attempted different combination of metals doped into TiO_2 under visible light irradiation [8]. Bakshayesh et al. studied on solar cell applications by using Sr and V co-doped TiO_2 nanomaterials due to easy incorporation of co-dopants into TiO_2 lattice causing grain strain resulting in smaller crystallite size and inhibiting the growth of rutile phase which are more advantageous for solar cell application [9].

Zn is found to be promised potential photocatalytic promoter basing on some of its merits such as firstly, the ionic radii of Zn^{2+} (0.74 A°) and Ti^{4+} (0.75 A°) are almost close to each other so more effective substitution of Ti^{4+} ion with Zn^{2+} takes place without disturbing the crystal structure, hence stabilizing the anatase phase [10]. Secondly, with Zn doping, the separation rate of the charge carriers was prolonged because of the introduction of an energy band just below the conduction band of TiO_2 [11]. Er and Mg co-doped TiO_2 were synthesized by Chen et al. via facile hydrothermal synthesis and applicated for photovoltaic property in perovskite solar cell [12]. Among all the alkali earth metals Mg^{2+} has proved to be a landmark dopant due to its ionic radius (0.72 A˚) similar to that of Ti^{4+} [13]. Other expedient role of Mg containing TiO_2 is in reducing the band gap by forming an extra energy level just above the valency band by overlapping of 2p orbital of Mg^{2+} and O^{2-} [14]. Based on the importance and involvement of Zn and Mg in reducing electron hole recombination and band gap as an individual dopant doped into TiO_2 lattice, in the present investigation, Zn and Mg co-doped TiO_2 were synthesized by sol gel method to fulfil above said both criteria.

However, enhanced surface area of a catalyst is a major contributing factor for effective photocatalytic activity. In the recent past, there are many capping agents assisted doped TiO_2 synthesis process were studied [15] but due to the rising concern regarding the biodegradability and long-term toxicity of these there is an urgency to develop an alternative green synthesis approach through biocapping as an ideal supplement [16].

By considering the above said facts, the present study proposed to use natural *Sapindus emerginatus* (Biogenic extract) as capping agent in the synthesis of Zn and Mg co-doped TiO_2.

Sapindus emerginatus (Soapnut) pericarp extract acts as a natural capping agent due to its major component saponin which in turn acts as a stabilizer and inhibits the agglomeration of doped TiO_2 to nano size which is a booster for effective photocatalytic degradation [17]. Ghaghi and his coresearchers demonstrated good Emulsification and Critical Micellar Concentration properties of it as compared to commercially available SDS surfactant [18]. In addition to saponins, the presence of phytochemicals such as flavonoids, glycosides, fatty acids and fixed oils makes it easier to use as biocapping agent [19].

Recently a great attention is emphasized on the effective degradation of Azo Dyes which constitute about 60-70% of all the textile and industrial dyes together which unique adverse toxic, mutagenic and carcinogenic properties create a threat to entire aquatic biota [20]. The present investigation envisages the visible light activity and catalytic efficiency of the synthesized catalyst evaluated by degradation of Amido Black 10B (AB 10B) dye as an exemplary pollutant. AB 10B is a classical azo dye consisting of sulphonic side chains. Pawaskar et al. noticed that the presence of these sulfonic groups makes it easily soluble and stable, making its treatment difficult by various conventional method [21]. So herein, the as synthesized Zn/Mg co-doped TiO_2 was successfully employed for degradation of AB 10B to corroborate its effective photocatalytic efficiency.

2. Experimental

2.1. Required chemicals and reagents

The main precursors of Titanium, Zinc and Magnesium, $Ti(OBu)_4$, $Zn(NO_3)_2.6H_2O$ and $Mg(NO_3)_2.6H_2O$ respectively were used for the synthesis of undoped and Zn/Mg co-doped TiO_2 catalysts. All the chemicals obtained were AR-Grade from E-Merck (Germany). AB 10B, an anionic textile dye pollutant was obtained from High media, India. *Sapindus emerginatus* (soapnut) extract was used as the biosurfactant for the synthesis of Zn and Mg co-doped TiO_2 (with surfactant). Ethanol and nitric acid are obtained from E-Merck (India) used as a solvent in the reaction procedure. All the above-mentioned chemicals were used as received and their solutions were freshly prepared using deionised water.

2.2. Extraction of soapnut pericarp

The fresh ripen fruit of soapnut was taken, shade dried and washed with deionised water and then 100 g of pericarp soaked in 100 mL of water for 6 h. Then the clear solution was filtered using Whatman filter paper No.1 and the aliquot (10%) was taken for further experimentation procedure.

2.3. Synthesis of Zn/Mg co-doped TiO_2

The synthesis co-doped TiO_2 catalysts was carried out using various weight percentage of dopants (Zn and Mg) by sol-gel method. In beaker 1, n-Butyl ortho titanate (20 mL) was dissolved in absolute alcohol (40 mL) and stirred for 10 min, acidified with 3.2 mL of nitric acid drop wise under continuous stirring for 30 min (Solution I). In another Pyrex glass beaker 2, 40 mL of ethanol, the calculated (required weight percentage 0.25-1.0 wt%) amount of dopants and 7.2 mL of water taken and continued stirring for 30 min (Solution II). This was followed by the slow dropwise addition of Solution II (from burette) to Solution I, under vigorous stirring until the transparent sol was formed, and stirring was continued for 2 h. The sol formed is kept aside for 48 h for aging in dark at room temperature to obtain gel. The gel was dried in an oven at 100°C and ground. The catalyst powder was calcined at 450°C in a muffle furnace for 5 h. The prepared catalysts were labelled as ZMT1, ZMT2, ZMT3, ZMT4 and ZMT5 as described in Table 1.

To select the best catalyst from the above prepared catalysts, assessment studies was conducted for degradation of AB 10B dye under visible light irradiation and the results were presented in Sec. 4.1 that suggests the best dopant concentration was obtained for ZMT4 with Zn (1.00 wt%) and Mg (0.25 wt%). For further boosting the photocatalytic performance of the ZMT4 catalyst, scissoring of the catalyst by using biogenic soapnut extract was carried out to control the agglomeration of the particles for getting smaller particle size resulting in enlarge surface area. Soapnut extract assisted ZMT4 nanocatalysts were synthesized by following the same procedure but varied volumes (5 mL, 10 mL, and 15 mL) of soapnut extract was added after the sol formation in the regular procedure and continued the stirring for 15 min and left the solution for ageing. Similar procedure was adopted for the synthesis of undoped TiO_2 (without addition of dopants and soapnut extract). Details of all the as synthesized catalysts are presented in Table.1.

2.4. Advanced instrumental techniques utilized for characterization of the catalyst

Powder X-ray diffraction (XRD) measurements were accomplished to determine the crystalline phase of pure TiO_2 and Zn/Mg co-doped TiO_2 in presence and absence of capping agent, using an X'PERT MPD_PRO diffractometer (Malvern Panalytical Ltd, Malvern, United Kingdom) with Cu Kα radiation operated at 45 kV, 40 mA and 0.2 theta scan rate (λ = 0.15405 nm). The average crystallite size of anatase form was determined according to the Scherer equation using FWHM data of the selected peak. Fourier-transform infrared (FTIR) spectra of the samples were recorded in frequency ranging from 4000–400 cm^{-1} using an FTIR spectrometer type JASCO 4100 (Jasco International, Tokyo, Japan) in transmission mode using KBr pellet method. UV–Visible diffuse reflectance spectroscopy (UV-DRS) with Shimadzu 3600 UV–Vis DRS Spectrophotometery in the range of 200–800 nm with $BaSO_4$ taken as a reference was used to determine the band gap of as synthesized catalysts. The morphology of the catalyst was studied using scanning electron microscope (ZEISS SIGMA FE-SEM) equipped with an energy dispersive X-ray Spectrophotometer and resolution 1 nm @ at 15 kV with HD. The size and shape of the nanoparticles were recorded with TECNAI FE12 Transmitted Electron Microscopy (TEM), operated current was 120 kV. The pore volume (V_P), size and surface area (S_{BET}) were determined by N_2 adsorption–desorption isotherm at 77.3 K using the instrument Brunauer-Emmett-Teller (BET) Quanta chrome Nova 2200 E System. Photoluminescence (PL) measurements was performed using Hitachi F-7000 fluorescence spectrophotometer. UV–vis spectrophotometer (Shimadzu 1601) was used to monitor the assays of AB 10B degradation during photocatalysis process. Elico digital pH meter (Model IIIE, EI) was used to monitor and adjust the pH of the reaction suspension during the degradation process.

2.5. Experimental setup and evaluation procedure for photocatalyic activity

The photocatalytic activity of the Zn and Mg co-doped TiO_2 nano material samples was evaluated by the degradation of AB-10B in a 150 mL pyrex glass beaker kept under continuous stirring in visible light irradiation. The photocatalytic procedure was given as follows: In a pyrex glass reaction beaker required

concentrations of catalyst and dye solution were taken. Before illumination, the mixtures were magnetically stirred under dark for establishment of adsorption/desorption equilibrium of AB-10B on the surface of catalyst. The high-pressure mercury metal halide lamp (400 W) with UV filter oriel no: 51472 was placed 20 cm away from the reaction mixture. To filter off IR radiation and to maintain the reaction condition at room temperature mixture was kept under running cool water which was circulated around the sample container. Prior to irradiation, the solution was adjusted to required pH by the addition of either 0.1N HCl or 0.1N NaOH. The rate of reaction was followed by withdrawing 5 mL aliquots of samples from the reaction mixture by using millipore syringe (0.45 µm) at different time increment and measure the absorption of the sample at λ max 619 nm by using UV-Vis spectrophotometer (Shimadzu 3600). The percentage of degradation of the dye (AB-10B) was calculated by using the following equation. % of Degradation = A_o-A_t/ A_o × 100, where A_o is initial absorbance of dye solution before exposure to light and A_t is absorbance of dye solution at time, t after exposure to light.

3. Results And Discussion

3.1. XRD

Powder XRD technique was utilised to analyze the structural properties of catalyst samples with and without surfactant and are shown in Fig. 2a and Fig. 2b. The 2θ values of each peak of all the catalysts were found at 25.3, 37.8, 47.9, 54.5, 57.1 and 62.5°, corresponding to (101), (004), (200), (105), (211) and (204) crystal planes of TiO_2 respectively, indicating the presence of anatase phase. The peaks almost coincide with undoped TiO_2 depicting the presence of dopants has no influence on anatase phase of TiO_2 calcined at 450 °C for 5 h [22]. This is may be due to the ionic radii of Zn^{2+} (0.74 A°) and Mg^{2+}(0.72 A°) are almost close to the ionic radii of Ti^{4+} (0.75A°), hence more effective substitution of both the dopants into TiO_2 lattice has occurred by substituting Ti^{4+} ions [10,13]. This can be further evident from the fact that no peaks at 2θ = 31.7, 34.5, 36.3, 47.5, 56.2 and 62.7° for ZnO and 2θ =36.7, 42.7 and 62.0° for MgO were observed [23, 24]. Further it is indicated that from the Fig. 2b the presence of intense and sharp peaks for ZMT4S2BC attributed to the effective capping of co-doped TiO_2 with biogenic surfactant [17]. Using Debye Scherrer equation (d = kλ/β Cosθ,) [25] average crystallite size of undoped, Zn/Mg codoped-TiO_2 and capped Zn/Mg codoped-TiO_2 were calculated, and presented in Table 2. From the table 2 it can be inferred that the crystallite size for capped ZMT4S2 (5.74 nm) is lesser than undoped ZMT4 (7.02 nm).

3.2. TEM

The particle size of the catalyst was analyzed by the TEM and the images were presented in Fig. 3a-f, which describe the surface morphology and particle size distribution of undoped TiO_2, ZMT4 and ZMT4S2. Fig. 3a depicts the nanospheres agglomerated particles of undoped TiO_2. Clear nanospheres with small particle size and less agglomeration for ZMT4 (Fig. 3b) and no agglomeration for ZMT4S2

(Fig. 3c) were observed. From the Guassian fitting method shown in inset of Fig. 3b and Fig. 3c ,the particle size distribution histograms was obtained which indicated that the average particle size of ZMT4 and ZMT4S2 was found to be 7.8 nm and 6.92 nm respectively. The decrease in the particle size of ZMT4S2 is may be due to the encapsulation of biogenic surfactant (capping agent) during the synthesis process. The HRTEM image (Fig. 3d) exhibited that the ZMT4S2 contained randomly oriented nanocrystals with anatase phase. The SAED pattern of ZMT4S2 (Fig. 3e) was also studied for the concentric rings attributed to the polycrystalline nature which is indicated by the (420), (204), (004), (226) and (215) anatase planes which are in good concordance with the XRD results. Moreover, the interplanar space determined for a tetragonal structure anatase 101 peak was found to be 0.302 nm (Fig. 3f).

3.3. FTIR analysis

Figure 4 displayed the FTIR spectrum of undoped TiO_2, ZMT4 and ZMT4S2BC. The spectra revealed the peak at 512 cm^{-1}, attributed to the stretching vibration of Ti-O-Ti of undoped TiO_2 which has been shifted to 490 cm^{-1} for all the doped samples implies the doping of Zn and Mg into TiO_2 framework by substituting Ti^{4+} ion [26]. The peaks at 1633 cm^{-1} related to H-O-H bending vibration, and the peaks at 3000–3400 cm^{-1}corresponding to the stretching vibration of the surface hydroxyl groups of O-H which is in good agreement with the literature reports [27]. No peaks observed at 457 cm^{-1} and broad peak in the range 3300–3600 cm^{-1} indicating the absence of ZnO and MgO, which coincides with the XRD results [28, 29]. The stretching frequencies observed at 1201 cm^{-1} and at 1065 cm^{-1} attributed to Zn-O-Ti and Mg-O-Ti which is evident for the substitutional doping of Zn and Mg by replacing Ti^{4+} ion in TiO_2 lattice [6, 30]. In addition to it, the peaks corresponding to the stretching frequencies of Saponins (Sapindus emerginatus pericarp) have been shifted when it encapsulated the catalyst particles. These results of saponins and flavonoids with respect to ZMT4S2 were presented in Table 2.

3.4 BET Surface area analysis

Figures 5a and 5b explained about the N_2 adsorption–desorption isotherms and BJH pore size distribution curves of ZMT4 and ZMT4S2 calcined at 450 °C, respectively. The bioextract have been explored for its potent capping properties and the plot exhibited a type IV isotherm with a type H_2 hysteresis (according to the IUPAC classification) which suggests that the sample is mainly classified as mesoporous [31] with enhanced surface area (195.20 m^2g^{-1}) of ZMT4S2 when compared to ZMT4 (132.01 m^2g^{-1}). The difference in surface area may be contributed from the effective capping derived from amphipolar characteristics of triterpenoid (major component of saponin) which in turn accounts for non-agglomeration and stability of as synthesized ZMT4 catalysts (in presence of biogenic surfactant) [19]. The increment in surface area follows the trend ZMT4S3<ZMT4S1<ZMT4S2 that can be analyzed from the fact that Sapindus saponin being a nonionic surfactant and the presence of bulkier terpenoid molecule is capable of showing capping property up to optimized surfactant concentration beyond which

the degree of interaction of hydrophilic groups with the TiO_2 lattice decreases due to more crowding which restricts the formation of micelles. Hence, increase in CMC (Critical Micellar Concentration) decreases the encapsulation [32].

3.5. UV–Vis-Diffuse reflectance spectroscopy

UV–vis DRS spectra of synthesized Zn/Mg co-doped TiO_2 around 400-500 nm showed a remarkable redshift in the wavelength as compared to undoped TiO_2 (Fig. 6a). This shift may be resulted from the substitutional doping of TiO_2 by Zn and Mg which was inturn caused by an extra energy level band formed above the valence band by replacing Ti^{4+} in TiO_2 by Mg^{2+} [33]. The mixing of Mg (2p) with O (2p) orbital which facilitate electron excitement in visible region [14]. In addition to this, the incorporation of Zn^{2+} contribute to the prolonged separation of charge carriers [11]. Further it was supported by the calculated band gap energies of the all synthesized catalysts using the Kubelka-Monk formalism plot and Tauc plot method as shown in Fig 6b. The undoped TiO_2 exhibited the band gap of 3.12 eV but for the co-doped TiO_2 samples showing the band gap ranging from 2.7 to 2.9 eV. Among all the co-doped samples ZMT4 exhibiting the lowest band gap energy, i.e., 2.7 eV. The results indicated co-doping of Zn and Mg made all the catalysts to be visible light active, by which more number of electron-hole pairs is generated by the absorption of visible light and leads to higher photocatalytic activity. Moreover, the addition of surfactant led to the further reduction in bandgap to 2.10 eV as depicted in Fig. 6d suggesting that oxygen deficiency displaying excellent sensitivity towards visible light and enhanced photocatalytic efficiency. The comparison results of bandgap of singly doped and surfactant assisted co-doped TiO_2 have been tabulated in Table 3.

3.6. SEM

Figure 7 shows the SEM images of undoped and ZMT4 clearly depicting the spherical shape with rough morphology and uneven distribution of particles indicating efficient doping of TiO_2 with Zn and Mg, which can be further confirmed from the EDX analysis. The EDX spectrum reveals the diffraction peaks corresponding to Zn at 1.00 and 8.75 keV and for Mg at 1.25 keV infers the successful doping of co-dopants. The overall data shows the atomic wt% of Zn and Mg which are in good concordance with the calculated value.

4. Envisage The Photocatalytic Performance Of Zmt4 And Zmt4s2 (After Calcination).

To explore the photo-degradability of AB 10B dye with ZMT4 and ZMT4S2 catalysts under visible light irradiation, a series of experiments were designed in order to determine the reaction conditions for complete degradation of dye. Before establishing the reaction conditions, trial experiments were conducted to know the sensitivity of dye and catalyst.

In the first trial, 100 mL of 5 mg/L AB 10B dye solution was taken in a 150 mL pyrex glass vessel without catalyst and exposed to light for 60 min. 5 mL of aliquots were withdrawn at different time intervals and measured the absorbance at λ_{max} of 619 nm. No appreciable change in the absorbance was observed for the dye solution before and after exposure to light implies that the insensitivity of dye towards light.

In 2nd trial, the reaction vessel containing dye solution (5 mg/L) with catalyst dosage (50 mg/L), maintained at pH=3 was stirred in the dark for 60 min and the aliquot taken was analyzed for absorbance at same λ_{max}, the small change in absorbance of the dye was observed indicating the adsorption of dye molecules on the surface of charged catalyst.

In the last trial, the reaction vessels containing above said components kept in visible light irradiation for 60 min under continuous stirring and at different time intervals the aliquots samples were taken and absorbance was measured. It is noted that the progressive decrease in absorbance was occur which attributes to the interdependence of light and catalyst.

Based on the above said conditions it is necessary to optimize the reaction conditions.

4.1. Optimization of reaction conditions

To determine the influence of dopant concentrations and efficiency of the catalyst, experiments were conducted at different dopant concentrations by keeping other parameters constant such as catalyst dosage 0.05 g/L, solution pH 3, and initial dye concentration 5 mg/L. The experimental results depicted in Fig. 8 clearly revealed that the photocatalytic behaviour of all the co-doped TiO_2 catalysts (ZMT1-ZMT5) are more pronounced than undoped-TiO_2, attributed to the narrowing of band gap as discussed in sec. 3.5. But among all the catalyst ZMT4 exhibit elevated rate of degradation which is ascribed to utmost decrease in bandgap of TiO_2 in ZMT4 and reduction in electron hole recombination. At higher concentration of dopants, they deposit on the surface of catalyst rather than substitution doping into TiO_2 lattice. This can provoke the acceleration of electron hole recombination which retard the rate of degradation [35]. Within these two dopants Mg^{2+} form an extra Fermi energy level by mixing of 2p orbitals of Mg and O. In the same way, Zn^{2+} facilitated as an electron trap by forming an extra energy level below the conduction band by mixing of 3d orbitals of conduction band and Zn^{2+} [11]. In view of decrease in band gap of each particle, high quanta of visible radiations were absorbed leading to high quantum efficiency.

Based on the above data ZMT4 (1.00% Zn and 0.25% Mg) found to be an effective photocatalyst and for further enhancement in the photocatalytic activity of ZMT4 two factors decrease in particle size and increase in surface area favours the enhancement process. To achieve this criteria, ZMT4 was re-synthesized in presence of biogenic surfactant at 3 different concentrations and the process was discussed in Sec.2.2.2. After calcination the catalytic efficiency of these three catalysts (ZMT4S1, ZMT4S2 and ZMT4S3) were evaluated and the results were shown in Fig. 9. Among these ZMT4S2

exerts highest photocatalytic activity than the other two because of the detrimental effect on further increasing the surfactant concentration causes the restriction for coherent doping of metal ions [36]. The rate degradation graph of these three catalysts is given in Fig. 9 as an inset. This result corroborated with the results obtained in XRD, TEM and BET surface area analysis (Sec 3.1,3.2 and 3.4). During the further course of catalysis ZMT4S2 fixed as a best catalyst and other parameters were varied for obtaining optimum conditions.

The impact of solution pH on the photocatalytic activity of ZMT4S2 for the degradation of AB 10B dye was studies by varying the pH from 2 to 9 and keeping the other parameters constant such as catalyst dosage (0.05 g/L) and dye concentration (5 mg/L). All the experimental results are shown in Fig. 10 shows that the degradation rate was observed to be high in acidic pH. Under acidic conditions <6.25, the surface hydroxyl group (Ti-OH) undergo protonation ($Ti\text{-}OH_2^+$) by making the surface positive which facilitate the adsorption of negatively charged AB 10B dye molecule by electrostatic interaction. Further, increase in pH from 5 to 6, the positivity of the surface decreases slowly and becomes negative by approaching 8 to 9 pH. On the whole, pH 3 is the better optimal condition where the surface of the catalyst is positive which is more favourable for the adsorption of negative dye molecule. Hence, at this condition, the rate of degradation is high. At pH 2, the approachability of the H^+ towards Ti-OH on the surface is more competitive due to repulsion between protons [30].

The Fig. 11 illustrates the photocatalytic activity of ZMT4S2 at different catalyst loading varying from 0.05 g/100 mL to 0.20 g/100 mL keeping other parameters constant. It is clearly observed that the catalyst dosage at 0.1 g/L exhibited highest rate of degradation, later it decreases by increasing catalyst dosage. This condition may be attributed to the greater availability of catalyst up to optimum concentration (100 mgL^{-1}) beyond which the increase in catalyst concentration the degradation rate decreases due to non-availability of the sufficient dye molecules to react with the active catalyst particle, also high catalyst dosage concentration, increases the turbidity impeding the penetration of light henceforth lowering the photocatalytic efficiency in the given working conditions [37].

After selection of the catalyst, pH and catalyst dosage, the final parameter initial dye concentration has to be optimized. Initial dye concentration varying from 5 mg/L, 10 mg/L and 15 mg/L by maintaining the other parameter constant. It can be inferred from the plot (Fig. 12) that the rate of degradation increases up to 10 mg/L dye concentration later it decreases (15 mg/L), this is may be attributed that up to 10 mg/L dye concentration, the surface area of photocatalyst is fully saturated with the monolayer deposition and simultaneous degradation of dye molecule but at high concentration (15 mg/L) due to blanket effect, multilayer adsorption penetration of light to the surface of the catalyst decreases [38]. Moreover, confinement of $^{\bullet}OH$ radicals at fixed catalyst dosage due to non-availability of catalyst particle confines the rate of degradation.

Optimum conditions for efficient degradation (99%) of Amido Black 10B by ZMT4S2 was arrived at catalyst dosage (0.1 g/L), dye concentration (10 mg/L) maintained at pH 3.

5. Identification Of Active Species Formed During Photocatalysis Using Scavenger Reagents

To draw the reaction mechanism for photocatalytic degradation of AB 10B by using ZMT4S2, there is a need to identify the reaction species using scavenger reagents.

In the present research article specific scavenging reagents were employed to identify the role of reactive species such as e^- holes, hydroxyl radicals ($^{\bullet}OH$), and superoxide radicals ($^{\bullet}O_2^-$) as shown in Table 5.

5.1. Assessing the role of e- holes and superoxide radicles

For this purpose, reaction medium consists of ZMT4S2 catalyst dosage (0.1 g/L), dye concentration (10 mg/L) maintained at pH 3 was taken in two separate beakers and carried out the reaction up to 5 min. Then in first beaker an effective hole trap EDTA was added and progress of reaction was monitored. The decrease in the % degradation up to 25% evident for the suppression of the holes generated. This indicates the presence of photogenerated e^- holes in the reaction. In the second reaction vessel the superoxide radical scavenger 1,4 Benzoquinone was added after 5 min of reaction. It resulted in the reduction of degradation up to 15% under given experimental condition indicates the formation of superoxide radical.

The results are represented in Fig. 13 a plot of % degradation v/s time.

5.2 Assessing the role of OH· radicle as reactive species.

To investigate for the production of $^{\bullet}OH$ radicle as reactive species photoluminescence studies were conducted using coumarine as a probe molecule which after reaction with hydroxyl radical forms, highly fluorescent 7-hydroxy coumarin in the reaction medium and the fluorescent intensity was measured at 450 nm. The corresponding obtained spectra was plotted PL intensity against wavelength and the outcomes were presented in Fig. 14. It can be inferred from the Fig. that the produced $^{\bullet}OH$ was in proportionate to the 7 hydroxy coumarine formed. The ZMT4S2 catalyst showed the presence of hydroxyl radical which after a course of irradiation decreases with time.

5.3. Plausible mechanism

Irradiation of Zn/Mg-TiO_2 with visible light excites an e^- from the valence band to the conduction band thus generating a hole on the valence band.

$$Zn/Mg\text{-}TiO_2 + hv \rightarrow Zn/Mg\text{-}TiO_2\ ({}_{VB}h^+) + Zn/Mg\text{-}TiO_2\ ({}_{CB}e^-)$$

$Zn/Mg\text{-}TiO_2\ (_{CB}e^-) + Zn^{2+} \rightarrow Zn/Mg\text{-}TiO_2 + Zn^+$

The holes thus generated reacts with the H_2O or surface hydroxyl group to form hydroxyl radical and H^+.

$Zn/Mg\text{-}TiO_2\ (_{VB}h^+) + H_2O \rightarrow Zn/Mg\text{-}TiO_2 + OH^- + H^+$

$Zn/Mg\text{-}TiO_2\ (_{VB}h^+) + OH^- \rightarrow Zn/Mg\text{-}TiO_2 + {}^{\bullet}OH$

The excited electron on conduction band reacts with the O_2 to produce super oxide radicals.

$Zn/Mg\text{-}TiO_2\ (_{CB}e^-) + O_2 \rightarrow Zn/Mg\text{-}TiO_2 + O_2^{-\cdot}$

The as produced superoxide radical reacts with H_2O producing hydroperoxy radical and hydroxyl ion.

$Zn/Mg\text{-}TiO_2\ (_{CB}e^-) + O_2^{-\cdot} + H_2O \rightarrow Zn/Mg\text{-}TiO_2 + HO_2^{\cdot} + OH^-$

The hydro peroxy radicals combine with H+ resulting in the formation of an intermediate product Hydrogen peroxide which in turn reacts with conduction band e^- to give hydroxyl radicals and hydroxyl ions.

$Zn/Mg\text{-}TiO_2\ (_{CB}e^-) + HO_2^{\cdot} + H^+ \rightarrow Zn/Mg\text{-}TiO_2 + H_2O_2$

$Zn/Mg\text{-}TiO_2\ (_{CB}e^-) + H_2O_2 \rightarrow Zn/Mg\text{-}TiO_2 + OH^{\cdot} + OH^-$

The ultimate formation of hydroxyl and superoxide radicles acts as a main reactive species for the degradation of dye adsorbed on the surface of catalyst.

$Dye + {}^{\bullet}OH \rightarrow$ Products

6. Recyclability Of Zmt4s2

In the present research scenario both the stability and efficiency of a catalyst are prominent features to account for the quality of catalyst. Based on this fact, our catalyst was active against AB10B dye up to 4 successive cycles with a decrement of 3% in each cycle with no appreciable loss of photocatalytic activity even after 4 cycles. Later the activity of catalyst tends to decrease appreciably with each cycle owing from the combination of factors including the substantial decrease in surface area and increase in rutile content when exposed to visible light or prolonged mechanical agitation. Also, rapid e- hole recombination owing to the increase in charge carriers deteriorates the photocatalytic activity of the catalyst [39].

7. Conclusions

This paper offers a great insight into the green synthesis of Zn/Mg-codoped TiO_2 assisted by capping agent i.e biogenic extract of Sapindus emerginatus pericarp via sol gel method. The complete strategical approach was designed to fully evaluate the potentiality of the as synthesized visible light driven Zn/Mg co-doped TiO_2 for degradation of AB 10B dye. Among the as synthesized catalysts, ZMT4 was found to be more efficient attributing to its polycrystalline rough spherical morphology with lattice planes coinciding with the XRD confirming pure anatase form of catalysts. The photocatalytic performance of ZMT4 was further promoted by Biocapping with different surfactant concentration (5 mL, 10 mL and 15 mL). Amongst them ZMT4S2 (10 mL) showed the best results with respect to decreased band gap (2.10 eV) crystallite size (5.74 nm) and surface area (195.20 $m^2 g^{-1}$). The TEM clearly demonstrates the comparative particle size distribution of ZMT4 and ZMT4S2 without any agglomeration. The characterization results further evident for photodegradability of AB 10B which was achieved 99% within 20 min of visible light irradiation. The scavenger test results conclude the presence of e^- holes, superoxide radicals ($\bullet O_2^-$) and hydroxyl radicals ($^{\bullet}OH$) as reactive species.

Declarations

Availability of data and materials

All data generated or analyzed during this study are included in this published article.

Competing interests

The authors declare that no competing interests

Funding

Not Applicable

Authors' contributions

GJ: conceptualization, experimentation, data interpretation and writing-original draft; TSR: supervision and writing-original draft; IMR: data interpretation and assisted in original draft writing, editing and revisions; GD and M.L.V.P.C: writing-review & editing. All authors read and approved the final manuscript.

Acknowledgement

G. Jaishree is thankful to Andhra Pradesh Pollution Control Board (APPCB), Andhra Pradesh for providing fellowship during this work. [Lr.No.APPCB/RFS/UH3/2019].

References

1. Zhang J, Xiao X, Nan J. Hydrothermal-hydrolysis synthesis and photocatalytic properties of nano-TiO_2 with an adjustable crystalline structure. J Hazard Mater. 2010;176:622–617.
2. Charitha T, Leshan U. Photocatalytic activity of N, Fe and Cu co-doped TiO_2 nanoparticles under sunlight. Curr Res Green and Sustain Chem. 2021;4:100186.
3. Adam K, Bielan Z, Bartkowiak A, Gabała E, Piasecki A, Zalas M, Zielinska-Jurek A, Janczarek M, Siwinska Ciesielczyk K, Jesionowski T. Synthesis of Titanium Dioxide via Surfactant Assisted Microwave Method for Photocatalytic and Dye-Sensitized Solar Cells Applications. Catalysts. 2020;10:586.
4. Zhuang H, Zhang Y, Chu Z, Long J, Xiaohan A, Zhang H, Lin H, Zhang Z, Wang X. Synergy of metal and nonmetal dopants for visible-light photocatalysis: a case-study of Sn and N co-doped TiO_2. Phys. Chem. Chem. Phys. 2016;18:9634–9636.
5. Abhijit K, Rohant D, Dongsu G, Kalyanrao G, Jinsub P. Sunlight driven high photocatalytic activity of Sn doped N-TiO_2 nanoparticles synthesized by a microwave assisted method. Ceram Int. 2017;46:5172–5164.
6. Ravi KM, Siva RT, Manga RI, Alim SA, Divya Lakshmi KV. Zinc and boron co-doped nanotitania with enhanced photocatalytic degradation of Acid Red 6A under visible light irradiation. Sustain Environ Res. 2019;29:29.
7. Aqeel M, Ikram M, Imran M, Ul-Hamid A, Qumar U, Shahbaz A, Ikramf M, Saeed A. TiO_2 Co-doped with Zr and Ag shows highly efficient visible light photocatalytic behaviour suitable for suitable for treatment of polluted water. RSC Adv. 2020;10:42248–42235.
8. Sankara RM, Siva RT, Alim SA. Study on Structural and Optical Properties of Ni and Mn Codoped TiO_2 Nanomaterials and Its Application in Visible Light Photocatalytic Activity of Indigo Caramine Dye. J Nanosci Tech. 2019;5:687–682.
9. Bakhshayesh AM, Bakhshayesh N. Enhanced short circuit current density of dye-sensitized solar cells aided by Sr, V co-doped TiO_2 particles. Mater Sci Semicond Process. 2016;41:101–92.
10. Dinkar A, Shridhar Jadhav S. Synthesis, characterization and photocatalytic applications of Zn-doped TiO_2 nanoparticles by sol–gel method. Appl Nanosci. 2016;6:972–965.
11. Jiang K, Zhang J, Rui L, Wan Y, Zengjian L, Jinwei Ch. A facile synthesis of Zn-doped TiO_2 nanoparticles with highly exposed (001) facets for enhanced photocatalytic performance. RSC Adv. 2021;11:7627.
12. Chen H, Zhu W, Zhang Z, Cai W, Zhou X. Er and Mg co-doped TiO_2 nanorod arrays and improvement of photovoltaic property in perovskite solar cell. J Alloys Compd. 2019;771:657–649.
13. Wang J, Nie Y, Miao Ch, Tan Y, Minyue W, Xiao W. Enhanced electrochemical properties of Ni-rich layered cathode materials via Mg^{2+} and Ti^{4+} co-doping for lithium-ion batteries. J Colloid Interface Sci. 2021;601:863–853.

14. Olowoyo JO, Kumar M, Singhal N, Jain SL, Babalola JO, Vorontsov A, Kumar U. Engineering and Modeling the Effect of Mg Doping in TiO_2 for Enhanced Photocatalytic Reduction of CO_2 to Fuels. Catal Sci Technol. 2018;8:3694–3686.
15. Radha DC, Siva RT. Synthesis of cobalt doped titania nano material assisted by gemini surfactant: Characterization and application in degradation of Acid Red under visible light irradiation. S Afr J Chem Eng. 2017;24:195–183.
16. Javed R, Zia M, Naz S, Aisida SO, Ul Ain N and Ao Q. Role of capping agents in the application of nanoparticles in biomedicine and environmental remediation: recent trends and future prospects. J Nanobiotechnol. 2020;18:172.
17. Swarnavalli GCJ, Dinakaran S, Raman N, Jegadeesh R, Carol P. Bio inspired synthesis of monodispersed silver nano particles using Sapindus emarginatus pericarp extract – Study of antibacterial efficacy. J Saudi Chem Soc. 2015;21:179–172.
18. Rupeshkumar G, Surekha SK, Balu CA, Arun BG. Study of functional properties of Sapindus mukorossi as a potential bio-surfactant. Indian J Sci Technol. 2011;4:233–231.
19. Balakrishnan S, Varughese S, Deshpande AP. Micellar Characterisation of Saponin from Sapindus Mukorossi. Tenside Surf Det. 2006;43:268–262.
20. Ben SH, Bouket AC, Zeinab P, Faizah AN, Silini A, Hafsa CS, Oszako T, Luptakova L, Golinska P, Belbahri L. Diversity of Synthetic Dyes from Textile Industries. Discharge Impacts and Treatment Methods. Appl Sci. 2021;11:6255.
21. Gokakakar SD, Pavaskar PA, Salker AV. Photocatalytic studies of Mn and Fe tetraphenyl porphyrins in the degradation of Amido Black 10B dye with solar light. SN Appl Sci. 2020;2:294.
22. Damkale RS, Sudhir AS, Govind UG, Sunit RB, Bharat KB. Highly crystalline anatase TiO_2 nanocuboids as an efficient photocatalyst for hydrogen generation. RSC Adv. 2021;11:7599–7587.
23. Abdelkhalek A, Abdulaziz A, Askar A. Green Synthesized ZnO Nanoparticles Mediated by Mentha Spicata Extract Induce Plant Systemic Resistance against Tobacco Mosaic Virus. Appl Sci. 2020;10:5069–5054.
24. ElNahhal M, Fawzi KS, Jamil SK, Hammad T, Kuhn S, Hempelmann R, Al BS. Silica, Mesoporous Silica and Its Thiol Functionalized Silica Coated MgO and $Mg(OH)_2$ Materials. Chem Africa. 2019;2:276–267.
25. Bokuniaeva AO, Vorokh AS. Estimation of particle size using the Debye equation and the Scherrer formula for polyphasic TiO_2 powder. J Phys: Conf Ser. 2019;1410:012057.
26. Ravi CM, Siva PRP, Siva RT, Pammi SVN, Siva KK, Vijay BK, Kiran KCh, Hemalatha KPJ. Enhanced visible-light photocatalysis and gas sensor properties of polythiophene supported tin doped titanium nanocomposite. J Phys Chem Solids. 2017;105:99–105.
27. Andrea L, Patricia R, Carolina G, Rodrigo S, Patricio V, Paula Z, Pedro A. FTIR and Raman Characterization of TiO_2 Nanoparticles Coated with Polyethylene Glycol as Carrier for 2-Methoxyestradiol. Appl Sci. 2017;7:58–49.

28. Sowri BK, Ramachandra RA, Sujatha Ch, Venugopal RK, Mallika AN. Synthesis and optical characterization of porous ZnO. J Adv Ceram. 2013;23:265–260.
29. Balakrishnana G, Velavana R, Mujasam Batoob K, Emad RH. Microstructure, optical and photocatalytic properties of MgO nanoparticles. Resul Phys. 2020;16:103013.
30. Balaram KA, Siva RT, Sreedhar B. Photocatalytic degradation of monocrotophos pesticide—An endocrine disruptor by magnesium doped titania. J Hazard Mater. 2011;186:1240–1234.
31. Elvira M, Coromelci CG, Lutic D, Vasile AI, Sacarescu L, Harabagiu V, Ignat M. Tailoring Mesoporous Titania Features by Ultrasound-Assisted Sol-Gel Technique: Effect of Surfactant/Titania Precursor Weight Ratio. Nanomaterials. 2021;11:1278–1263.
32. Rai S, Acharya-Siwakoti E, Kafle A, Devkota HP, Bhattarai A. Plant-Derived Saponins: A Review of Their Surfactant Properties and Applications. Sci. 2021;3:53–44.
33. Athira K, Merin KT, Raguram T, Rajni KS. Synthesis and characterization of Mg doped TiO_2 nanoparticles for photocatalytic applications. Mater Today: Proc. 2020;33:2327–2321.
34. Razali NA, Othman SA. Potential Dopant in Photocatalysis Process for Wastewater Treatment-A Review. IOP Conf Ser: Earth Environ Sci. 2021;736:012059.
35. Vargas HJ. Structural and Morphological modification of TiO_2 doped metal ions and investigation of photo-induced charge transfer processes, Physics [physics]. Université du Maine: Instituto politécnico nacional (México); 2017.
36. Strokova V, Gubareva E, Ogurtsova Y, Fediuk R, Zhao P, Vatin N, Vasilev Y. Obtaining and Properties of a Photocatalytic Composite Material of the "SiO_2–TiO_2" System Based on Various Types of Silica Raw Materials. Nanomaterials. 2021;11:892–866.
37. Nguyen AT, Juang RS. Photocatalytic degradation of p-chlorophenol by hybrid H_2O_2 and TiO_2 in aqueous suspensions under UV irradiation. J Environ Manage. 2015;147:277–271.
38. Chiu YH, Chang TM, Chun-Yi Ch, Sone M, Yung-Jung H. Mechanistic Insights into Photodegradation of Organic Dyes Using Heterostructure Photocatalysts. Catalyst. 2019;9:462–430.
39. Sorathiya K, Biswajit M, Abhishek K, Prabhakar RK, Gopinath ChS, Deepa K. Enhancement in Rate of Photocatalysis Upon Catalyst Recycling. Sci Rep. 2016;6:35084–35075.

Tables

Table 1

Details of all the samples synthesized

Serial number	Weight percentages of dopants (wt%)	*Sapindus emerginatus* surfactant (Volume in mL)	Name assigned to the sample
1	NIL	-	UTO (Undoped TiO_2)
2	0.25 Zn/0.75 Mg	-	ZMT1
3	0.50 Zn/0.50 Mg	-	ZMT2
4	0.75 Zn/0.25 Mg	-	ZMT3
5	1.00 Zn/0.25 Mg	-	ZMT4
6	1.00 Zn/0.50 Mg	-	ZMT5
7	1.00 Zn/0.25 Mg	5	ZMT4-S1
8	1.00 Zn/0.25 Mg	10	ZMT4-S2
9	1.00 Zn 0.25 Mg	15	ZMT4-S3

Table 2

Comparative stretching frequency values of pericarp extract and ZMT4S2BC.

S.No	Compound prepared	Stretching frequencies to be measured for	Frequencies/cm^{-1}	
			Frequency values for Soapnut Pericarp extract	Shifted frequency values for ZMT4S2BC (before calcination)
1.	*Sapindus emerginatus* pericarp [25]	O–H stretching vibration of flavonoids	3407	3412 (broad band)
		carboxylic O–H bond stretching vibration of saponins	2875	2994
		carboxylic C=O bond stretching vibration of saponins		
		C=O stretching vibration of flavonoids	1618	1633
		carboxylic O–H bending vibration of saponins		
			1693	1764
			1050	1376

Table 3

Comparative band gap values of Zn and Mg single doped, Zn/Mg co-doped TiO_2 and surfactant assisted Zn/Mg co-doped TiO_2.

S.No.	Catalyst	Bandgap (eV)
1	Zn doped TiO_2 [11]	3.1
2	Mg doped TiO_2[34]	2.9
3	Zn and Mg doped TiO_2 (Present work)	2.7
4	Surfactant assisted Zn and Mg codoped TiO_2 (Present work)	2.1

Table 4

Comparative Crystallite size, Bandgap, Surface area, Pore size and Pore volume values of all synthesized catalysts.

Serial number	Nanomaterials	Crystallite size (nm)	Bandgap energy (eV)	BET surface analysis		
				Surface area ($m^2 g^{-1}$)	Pore volume ($cm^3 g^{-1}$)	Pore size (nm)
1	Undoped TiO_2	32.50	3.2	74.32	0.12	48.4
2	ZMT1	8.03	2.9	114.45	0.21	57.0
3	ZMT2	7.90	2.85	122.57	0.22	60.8.
4	ZMT3	7.53	2.8	124.00	0.20	61.2
5	ZMT4	7.02	2.7	132.01	0.23	63.2
6	ZMT5	8.20	3.0	86.80	0.14	52.4
7	ZMT4-S1	6.40	2.25	158.62	0.25	68.5
8	ZMT4-S2	5.74	2.10	195.20	0.29	87.5
9	ZMT4-S3	7.40	2.5	122.85	0.25	73.3

Table 5

Specific scavenging reagents used for identification of reactive species

S.No.	Reactive species	Scavenging Reagents
1.	e^- holes	EDTA
2.	Superoxide radicals ($^{\bullet}O_2^-$)	1,4 Benzoquinone
3.	Hydroxyl radicals ($^{\bullet}OH$)	Coumarine

Figures

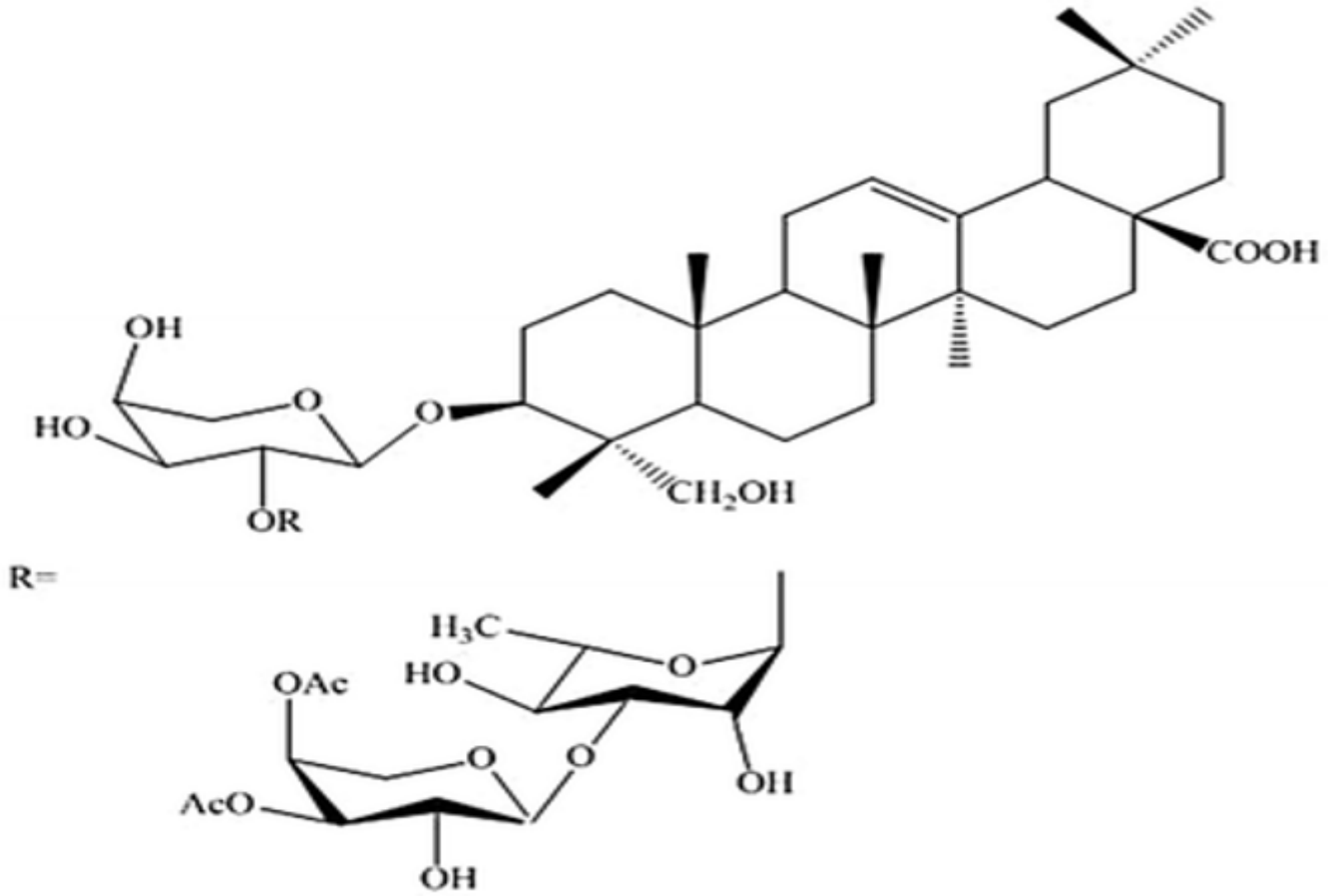

Figure 1

Structure of *Sapindus emerginatus* (Triterpenoid Saponin)

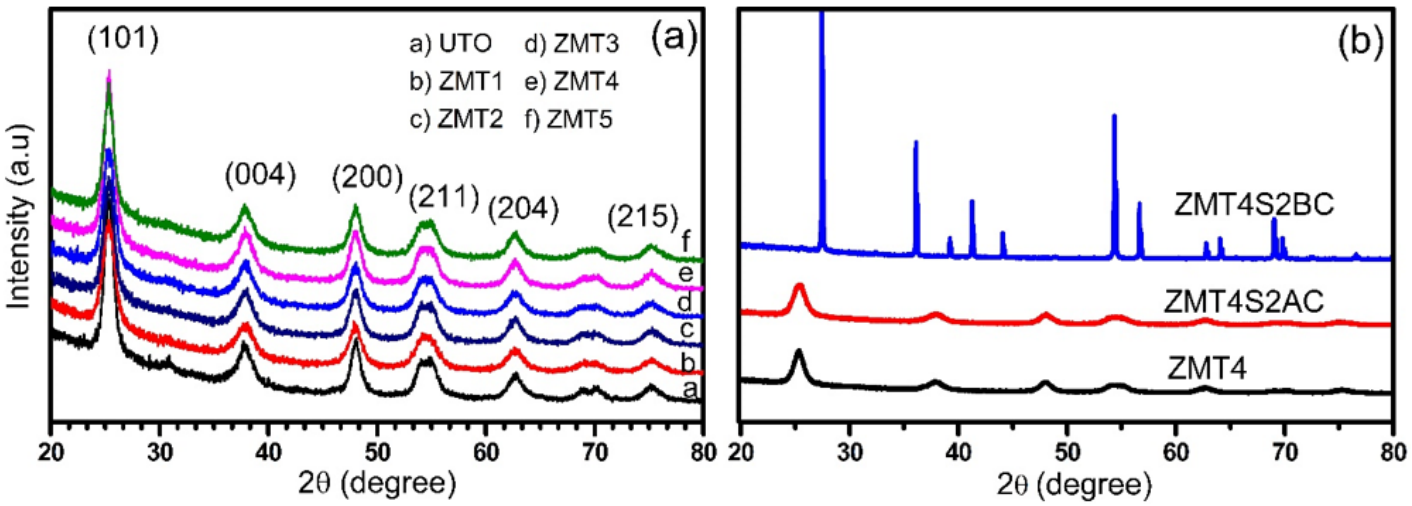

Figure 2

XRD pattern of a) undoped and Zn/Mg-co-doped TiO_2 (different wt%) b) ZMT4 and ZMT4S2 (before and after calcinations)

BC-Before calcination

AC- After calcinations

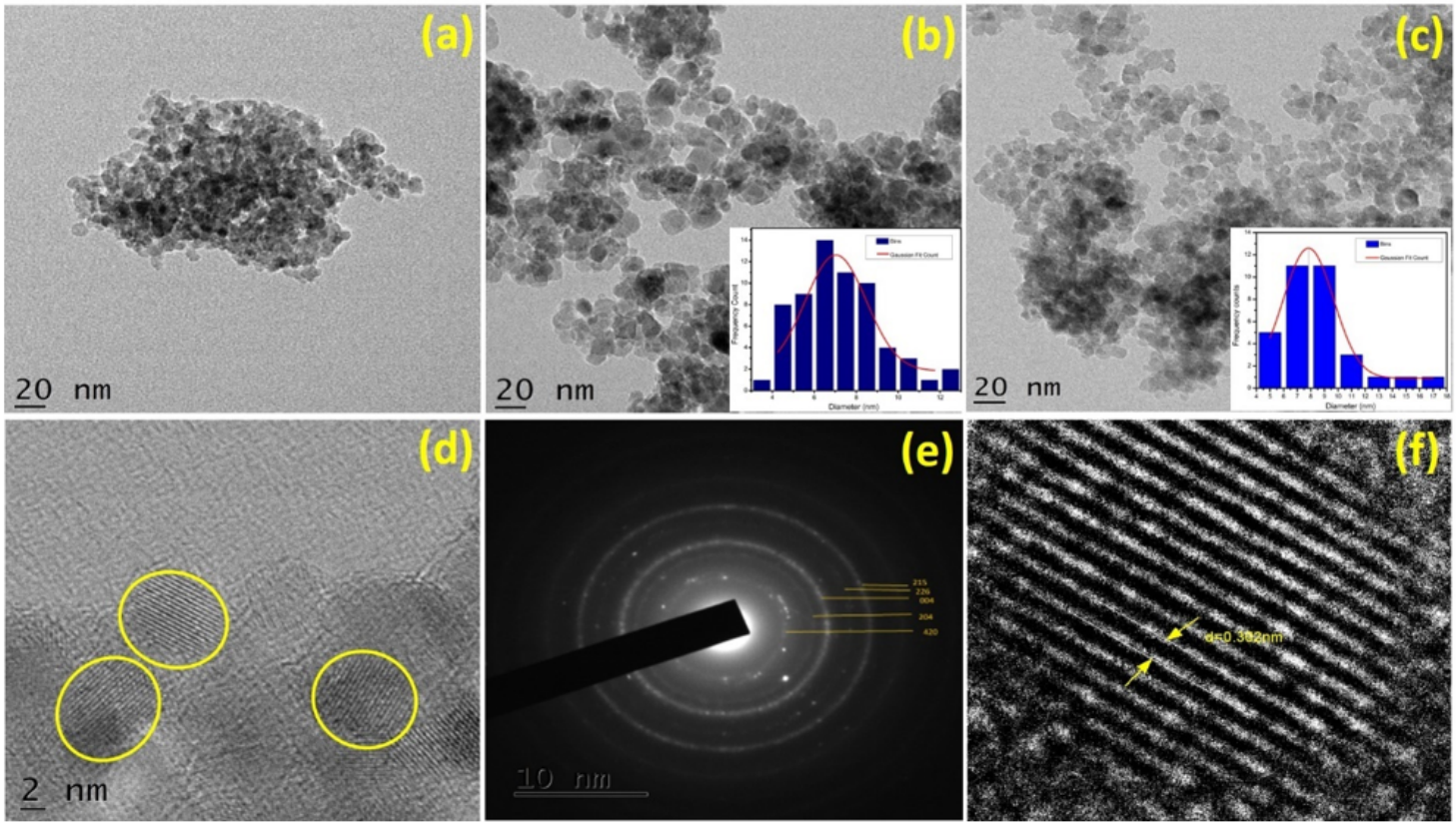

Figure 3

TEM micrograph of a) UTO, b) ZMT4, c) ZMT4S2, d) HRTEM image of ZMT4S2, e) SAED pattern and f) lattice fringes of ZMT4S2

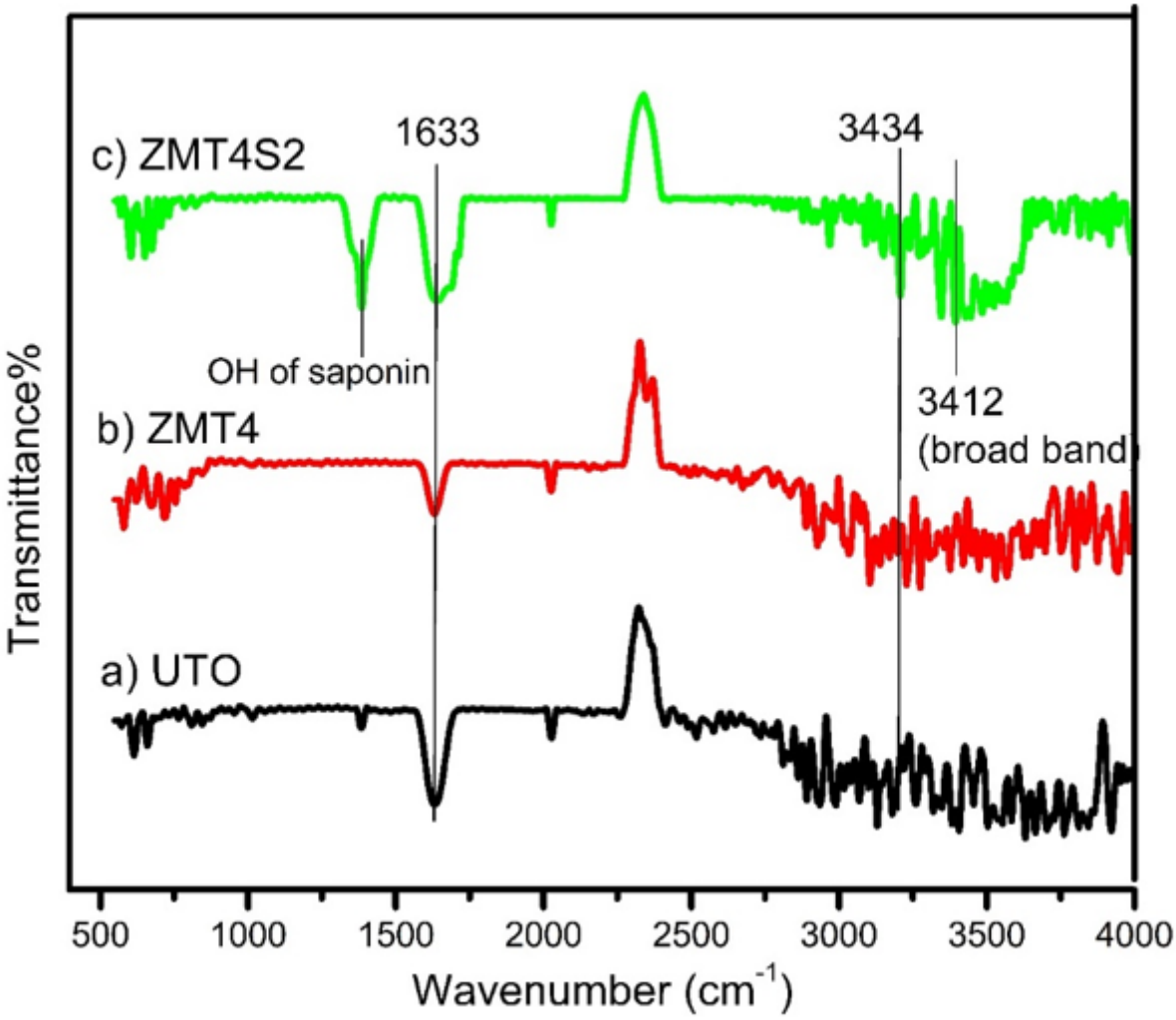

Figure 4

FTIR spectra of a) UTO, b) ZMT4 and c) ZMT4S2BC

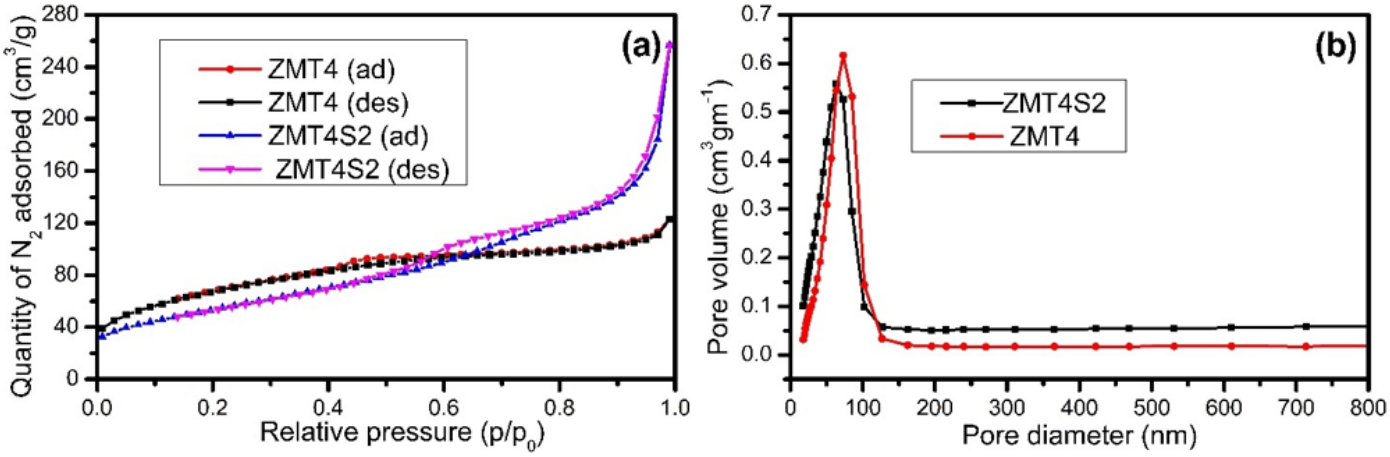

Figure 5

a) N_2 adsorption–desorption isotherms and b) BJH pore size distribution curves of ZMT4 and ZMT4S2

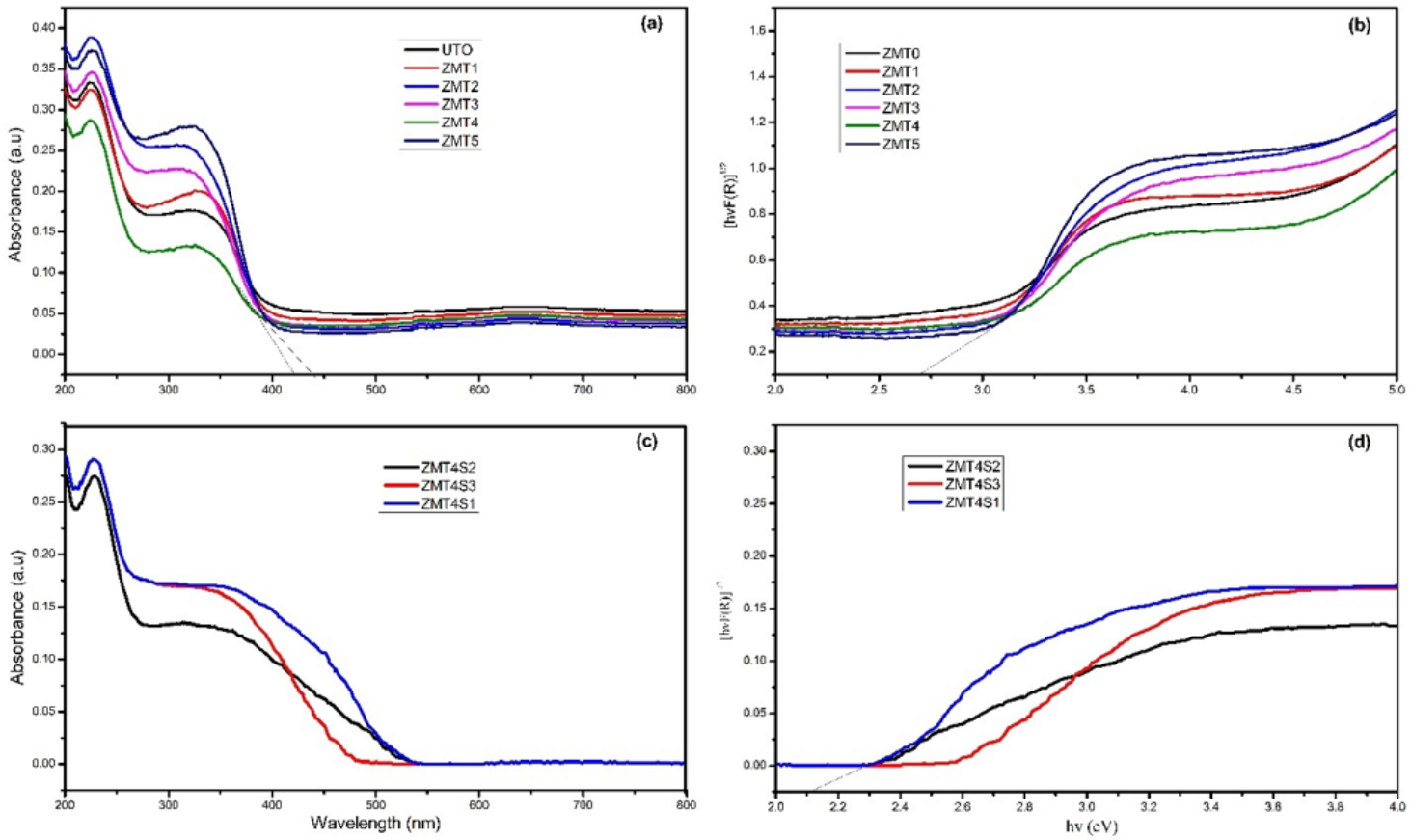

Figure 6

(a,c) The DRS spectra and (b,d) plots of transformed square root of Kubelka-Munk functions of Undoped and Zn/Mg co-doped TiO_2 without surfactant and with surfactant respectively.

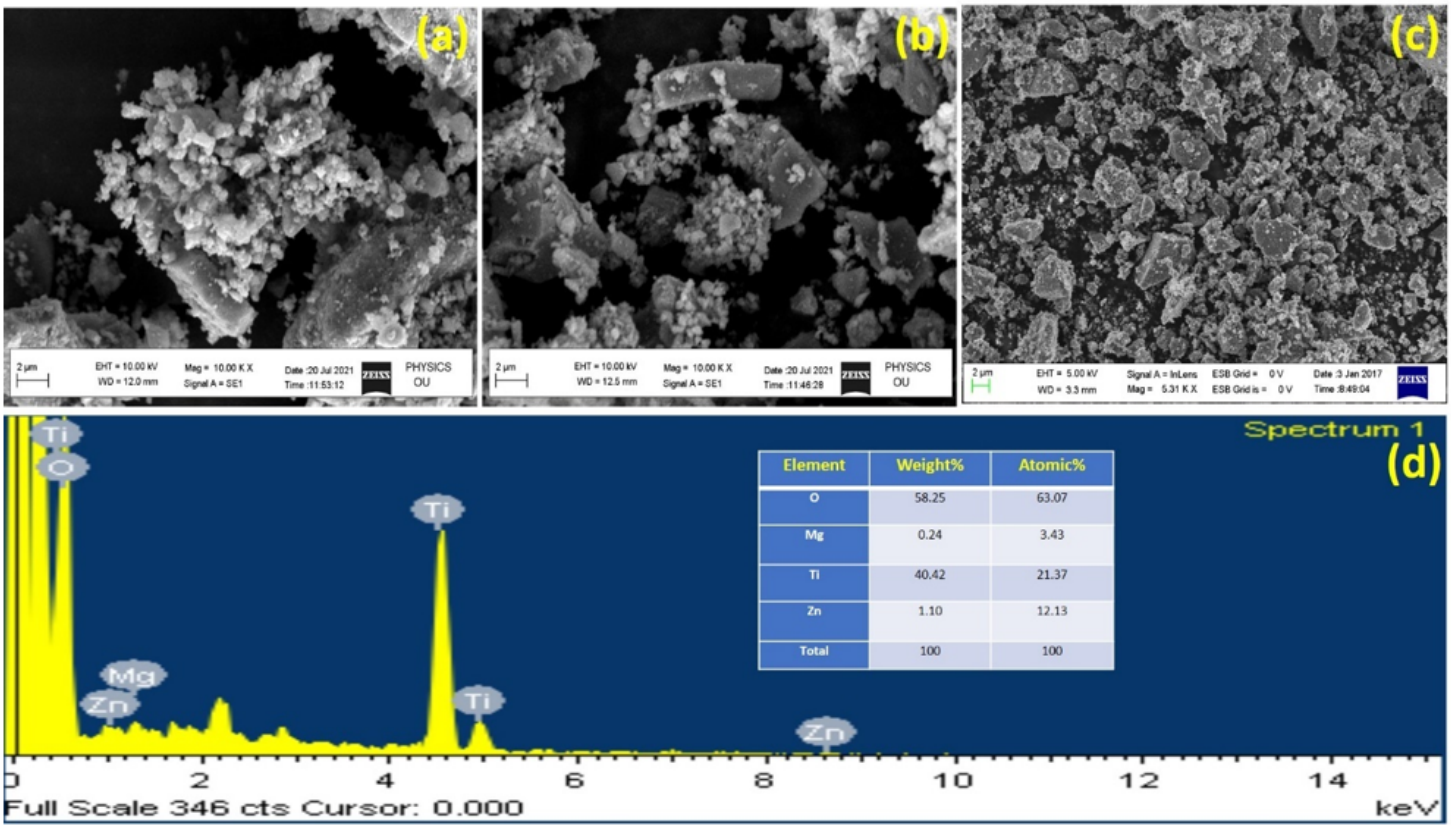

Figure 7

a) FESEM images of undoped TiO_2, b) ZMT4, c) ZMT4S2 and d) EDX spectrum of ZMT4.

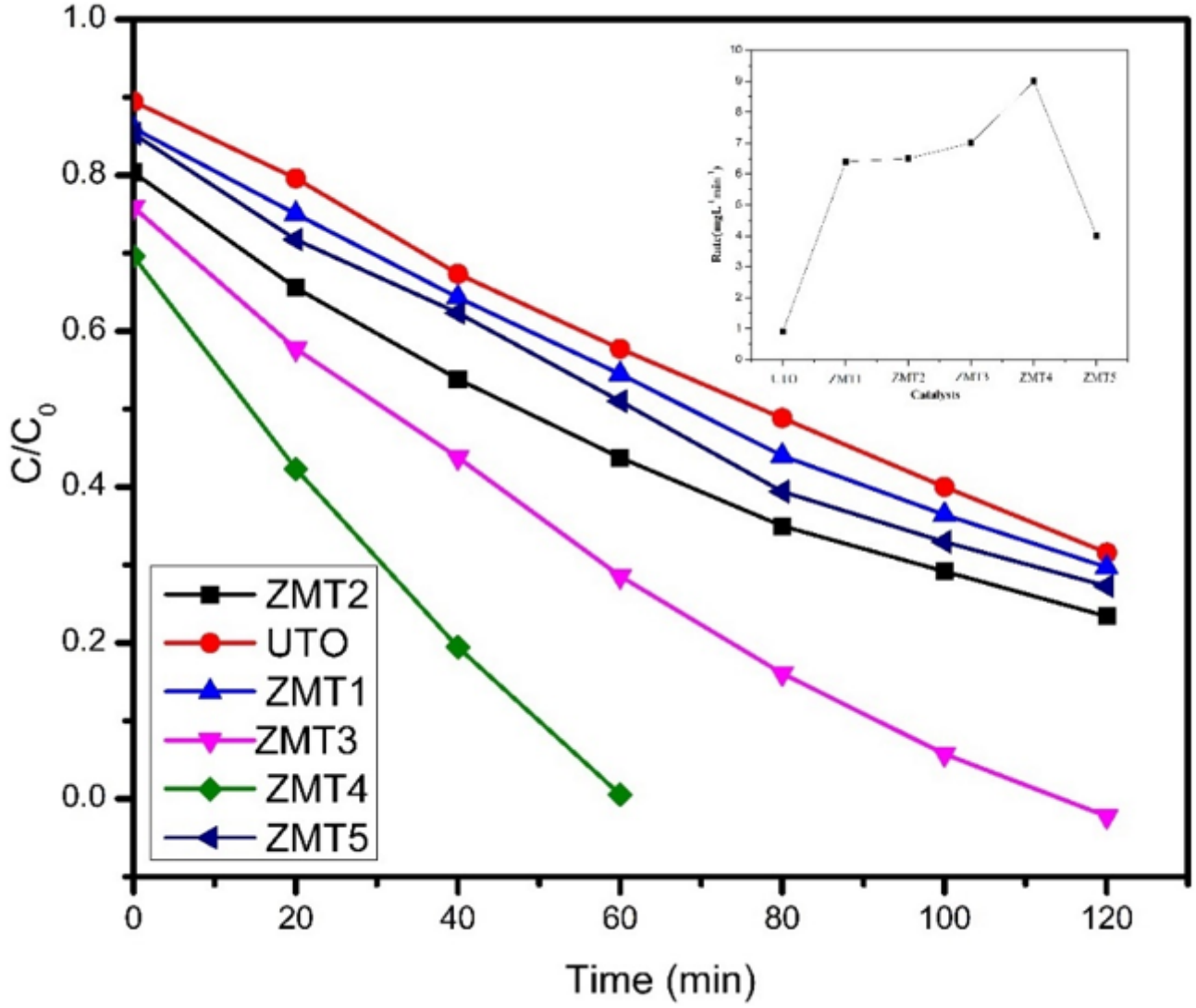

Figure 8

shows the effect of dopant concentration on degradation of Amido Black 10B. (catalyst dosage 0.05 g/L, solution pH 3, and initial dye concentration 5 mg L^{-1})

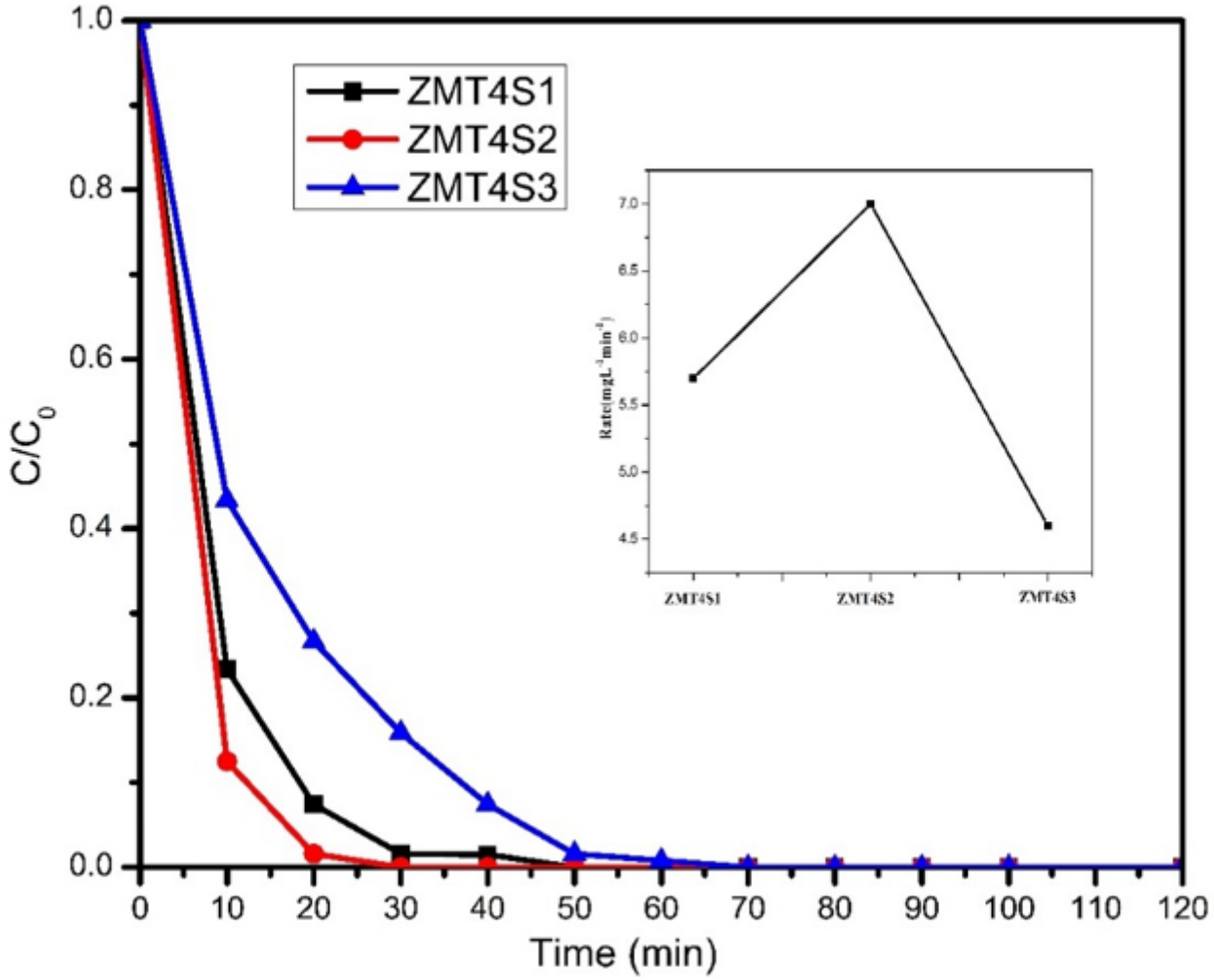

Figure 9

shows the effect of surfactant concentration on degradation of Amido Black dye

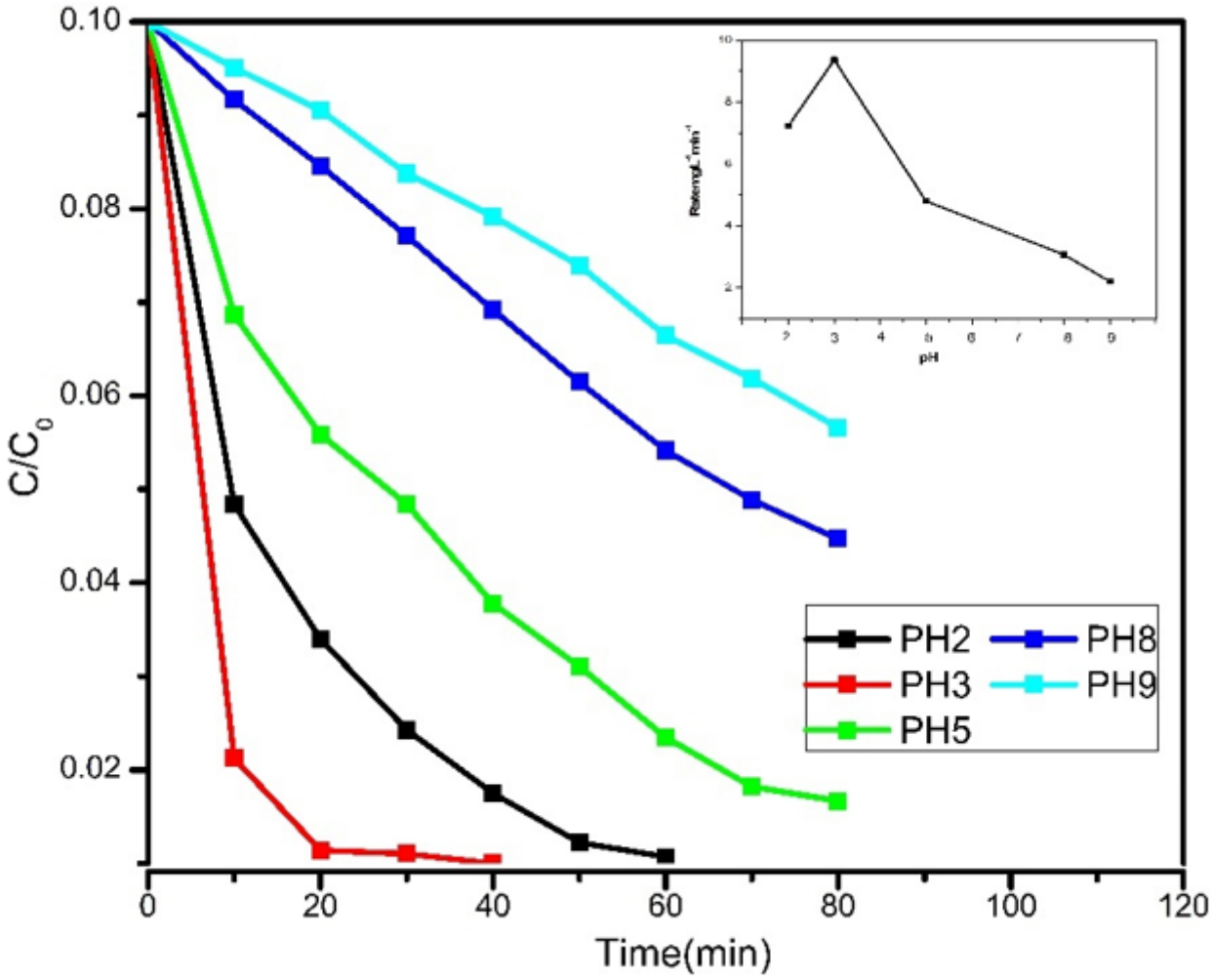

Figure 10

Shows the impact of solution pH on the degradation of Amido Black 10 B dye

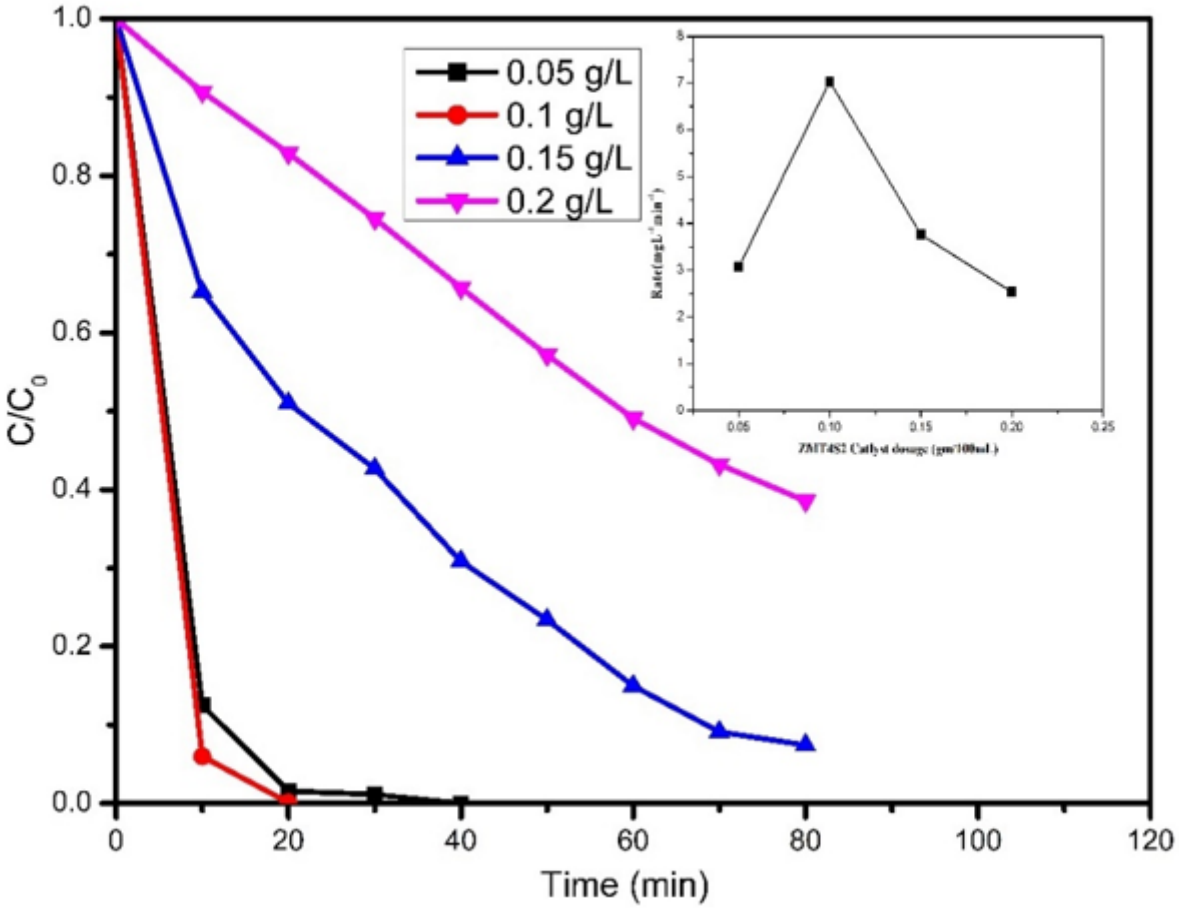

Figure 11

shows the impact of catalyst loading on degradation of AB 10 B

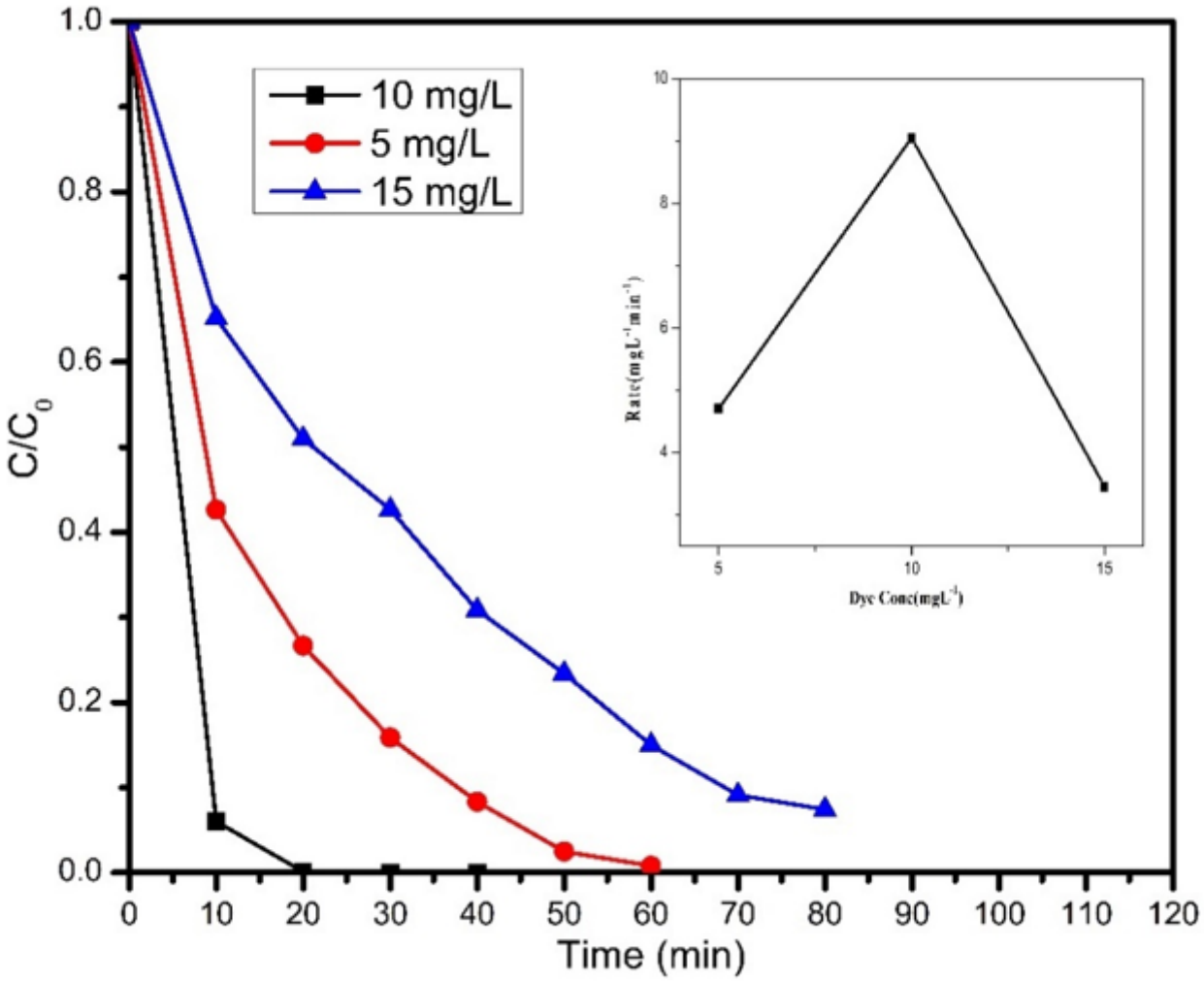

Figure 12

The effect of initial dye concentration on AB 10 B degradation

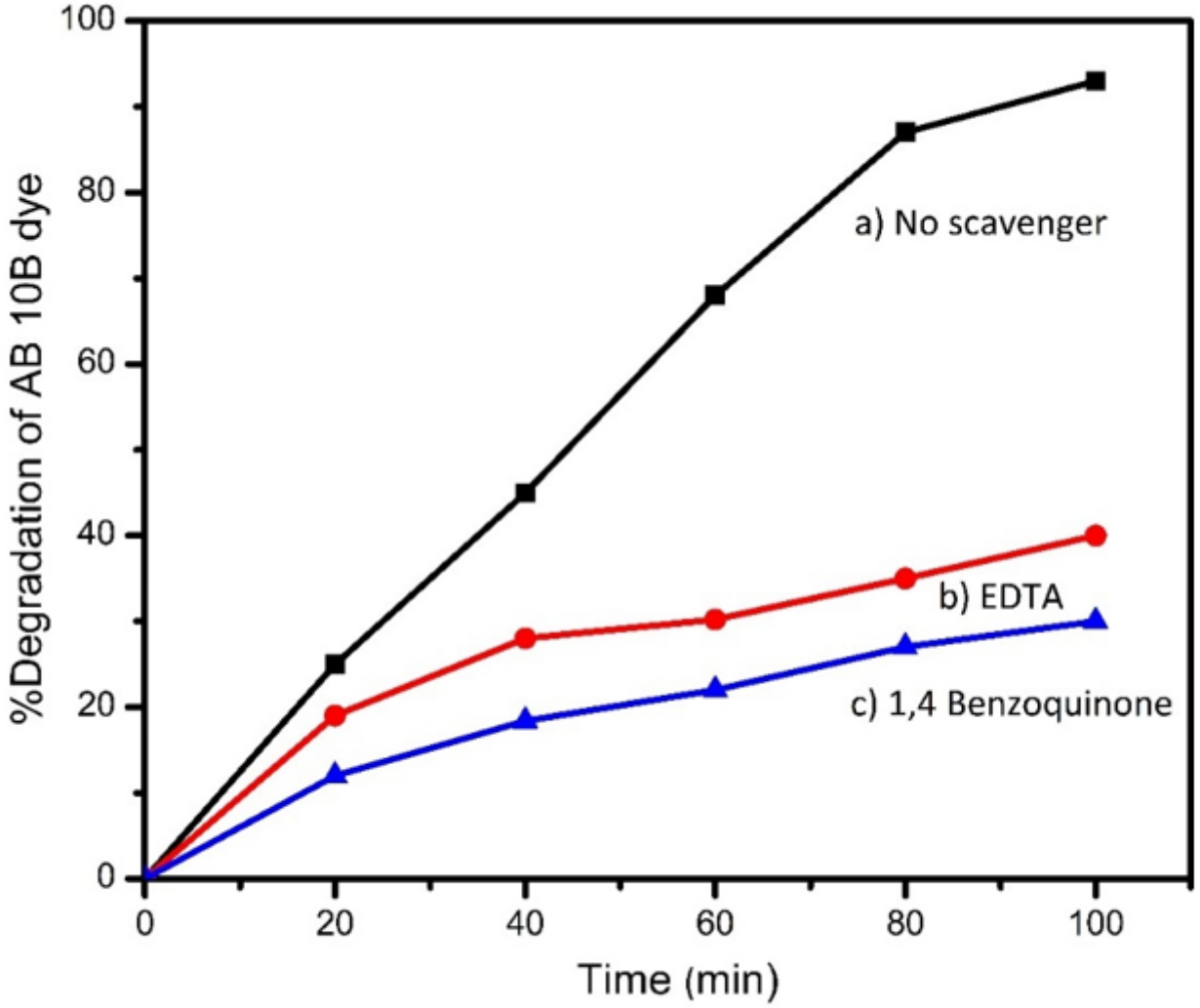

Figure 13

Effect of e^- hole and superoxide radicals ($^{\bullet}O_2^-$) scavenger on AB 10B degradation

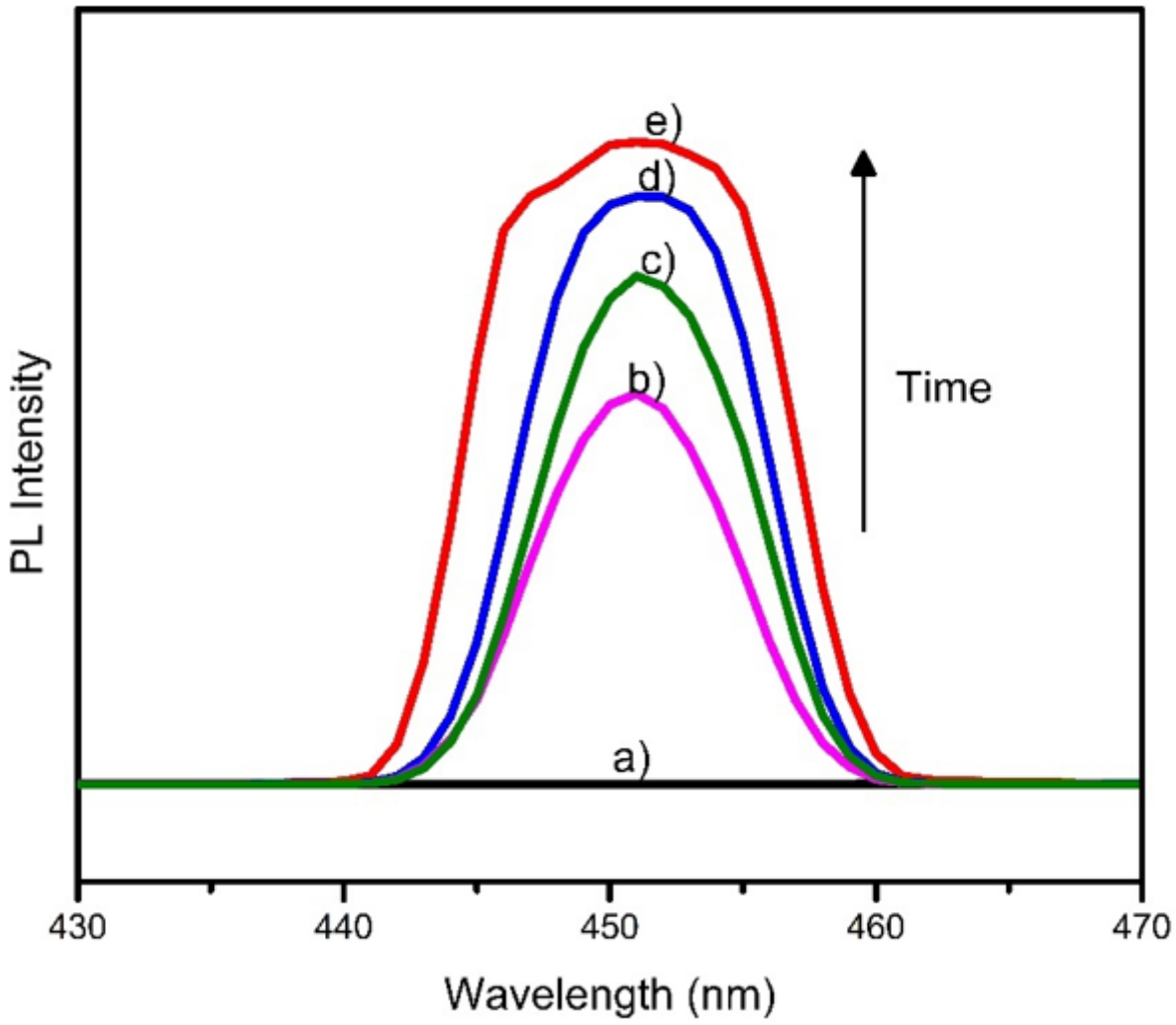

Figure 14

Photoluminescence Spectra of ZMT4S2, catalyst dosage (0.1 g/L), dye concentration (10 mg/L), pH 3

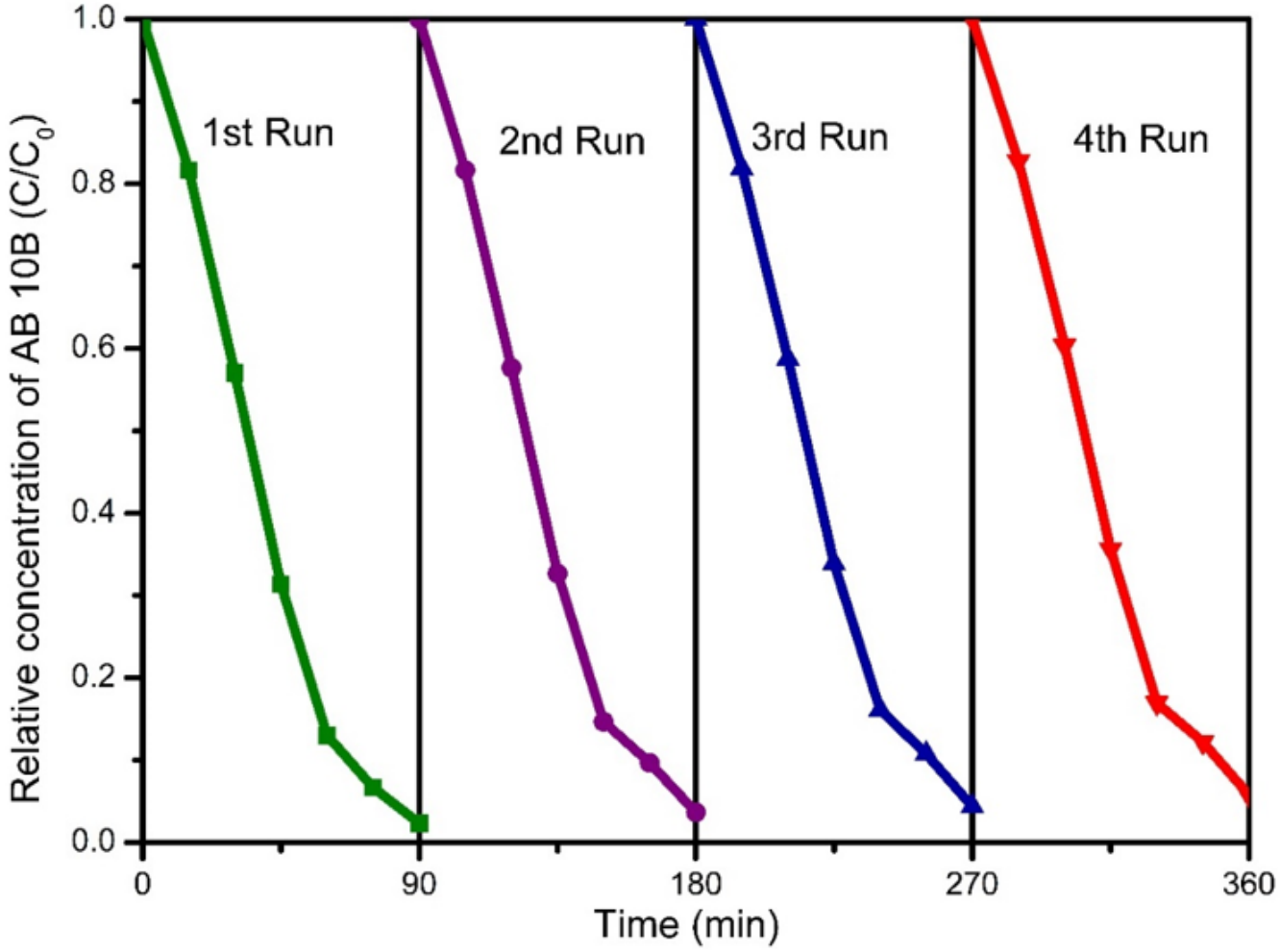

Figure 15

Recyclability test for ZMT4S2